ELSEVIER

Remote Sensing of Environment 81 (2002) 45–57

Remote Sensing of Environment

www.elsevier.com/locate/rse

Deriving green crop area index and canopy chlorophyll density of winter wheat from spectral reflectance data

N.H. Broge[a,*], J.V. Mortensen[b]

[a]Department of Agricultural Systems, Danish Institute of Agricultural Sciences, Research Centre Foulum, PO Box 50, Tjele DK-8830, Denmark
[b]Department of Crop Physiology and Soil Science, Danish Institute of Agricultural Sciences, Research Centre Foulum, PO Box 50, Tjele DK-8830, Denmark

Received 14 November 2000; received in revised form 29 October 2001; accepted 30 October 2001

Abstract

Spectral vegetation indices (VIs) are frequently used to estimate the amount of live green canopy material. They have generally been developed as an attempt to reduce spectral effects caused by external factors such as the atmosphere and the soil background. The objective of this study is to compare the performance of selected VIs, including some hyperspectral VIs based on waveform analysis of the reflectance across the vegetation red edge. The analysis is based on biophysical data measured in a winter wheat field fertilized at three nitrogen (N) levels. The measurements were acquired continuously throughout the growing season and related to canopy spectral reflectance measured with a ground-based spectroradiometer. Green crop area index (GCAI) and canopy chlorophyll density (CCD) were the major variables determined from the biophysical data set. Canopy chlorophyll was measured using nondestructive methods based on two optical instruments. The prediction power of selected VIs calculated from spectra resampled to Landsat TM configuration was compared with narrow-band indices including some VIs based on waveform analysis techniques. It was concluded that an exponential relationship exists between the two biophysical parameters and all of the selected indices except for the simple ratio index (RVI), for which a linear relationship was formed. The results indicate that VIs based on waveform analysis using narrow bands across the red edge may improve the prediction of CCD. However, none of the hyperspectral indices that were included in the study was better at estimating GCAI than the best of the traditional VIs.

1. Introduction

Spectral reflectance of vegetation in the 400- to 700-nm region is primarily governed by the abundance of chlorophyll and other pigments absorbing most of the incident radiation (Thomas & Gausman, 1977). However, in the spectral range 700–1300 nm, plants appear very bright, although leaf water produces a minor absorption peak at 970 nm and a more pronounced absorption peak at 1200 nm.

Spectral vegetation indices (VIs) calculated as combinations of near infrared (NIR) and red reflectance have shown to be well correlated with canopy parameters related to chlorophyll and biomass abundance such as green leaf area index (GLAI) and absorbed photosynthetically active radiation (APAR) (Elvidge & Chen, 1995; Myneni & Williams, 1994). Developments in the field of imaging spectrometry have fostered a new group of VIs based on the shape and relative position of the spectral reflectance curve. Collins (1978) and, more recently, Baret, Jacquemoud, Guyot, and Leprieur (1992), Demetriades-Shah, Steven, and Clark (1990), Filella and Peñuelas (1994), and Mauser and Bach (1995) concluded that derivative spectral indices are very sensitive to GLAI and chlorophyll concentration, while they tend to minimize spectral noise caused by the soil background and by atmospheric effects. GLAI is a key variable when modeling surface evaporation and biomass production (Moran, Maas, & Pinter, 1995), as well as yield (Bouman, 1992) and yield loss (Bouman, 1995; Hansen, 1991). Green crop area index (GCAI) is another measure of light interception. It is equivalent to GLAI but considers all green and thus photosynthetically active components of the plant including the area of green stems and ears. GCAI has been used to drive crop models such as the FASSET model (Jacobsen et al., 1998) for simulations of nitrogen (N) turnover and crop production at farm scale and for the estimation of growth rates and N status (Olesen et al., submitted).

* Corresponding author.
E-mail address: nielsh.broge@agrsci.dk (N.H. Broge).

0034-4257/01/$ – see front matter
PII: S0034-4257(01)00332-7

Canopy chlorophyll density (CCD) has been shown to be very sensitive to N availability in the soil (Hinzman, Bauer, & Daughtry, 1986). Thus, it can be used as a sensitive indicator of N deficiency, a problem common to field crops. Typically, N deficiency will cause leaf chlorosis, reduced net assimilation and growth rates, as well as lower GLAIs and grain yields (Osman, Goodman, & Cooper, 1977).

The objective of the present study is to evaluate the potential of a range of spectral reflectance-based approaches to quantify greenness of a winter wheat canopy. We define greenness in terms of GCAI (total area of green foliage per unit ground area) and CCD (total amount of chlorophyll present in the canopy per unit ground area). Prediction accuracies associated with commonly used satellite-based VIs are compared with those of narrow-band hyperspectral VIs recently proposed in the literature. As a part of the analysis, broad- and narrow-band versions of the traditional satellite-based VIs are also compared.

2. Materials and methods

The experiment was conducted as an open-field experiment at the main research facility of the Danish Institute of Agricultural Sciences. The soil type is classified as Dystic Luvisol by FAO (ISSS Working Group RB, 1998). It is characterized as a loamy sand with low base saturation throughout the soil profile and an organic matter content in the topsoil of approximately 3.5%. A soft winter wheat (*Triticum aestivum* L., variety Hussar) was planted on September 20, 1996 using 225 kg seed grain/ha and 12-cm row spacing. This variety does not develop awns, which can affect reflectance properties of some wheat varieties at the time of inflorescence. Three plots (10×20 m) representing three different N fertilization levels were established before the onset of the 1997 growth season. The N fertilization levels were 40, 80, and 120 kg N/ha. The normal N fertilization rate for this crop is 140–160 kg N/ha. However, the maximum fertilization level in this experiment was lower than normal in order to avoid lodging and ensure that effects of different N fertilization rates were not obscured by N saturation. The application rates and crop grain yield for each of the three plots are listed in Table 1.

Table 1
Fertilizer treatment and yield of the three soft winter wheat (variety Hussar) plots

Field plot	Date	W40N	W80N	W120N
(1) N treatment	4/4/1997	40 kg/ha	80 kg/ha	80 kg/ha
(2) N treatment	4/28/1997	–	–	40 kg/ha
Grain yield		3.37 tons/ha	5.02 tons/ha	5.92 tons/ha

The national yield average for winter wheat was 7.24 tons/ha in 1997.

2.1. Sampling and GCAI

Destructive samples (0.25 m^2) were taken weekly within each plot throughout the growing season in the harvest year (1997). The samples were taken in pairs with one from each side of the field plot. In the laboratory, the samples were divided into fractions of green leaves, semigreen leaves, yellow leaves, stems, ears, and weeds. The fresh weight, dry weight, and one-sided projected area of each fraction were then measured (Licor 3100 planimeter; LI-COR, Lincoln, NE, USA). The GCAI is defined as the normalized sum of the green leaf area (AGL), green stem area (AGS), and green ear area (AGE). Since only the leaf area was divided into green, semigreen, and yellow fractions, AGS and AGE were estimated from the total area of stems and ears (AS and AE) weighted by the green, semigreen, and yellow leaf areas (AGL, ASGL, and AYL) as suggested by Olesen et al. (accepted). The mathematical formulation is (Eq. (1)):

$$\mathrm{GCAI} = \mathrm{AGL} + (\mathrm{AS} + \mathrm{AE}) \times \left(1 - \frac{\mathrm{ASGL} + \mathrm{AYL}}{\mathrm{AGL} + \mathrm{ASGL} + \mathrm{AYL}}\right) \quad (1)$$

This formulation implies that the green proportion of stems and ears is assumed to be the same as for leaf lamina. Finally, the results from each pair of samples were averaged to obtain a mean plot value in order to minimize the effects of variability within the plots.

2.2. Leaf chlorophyll content (LCC)

2.2.1. Nondestructive measurements of leaf chlorophyll

LCC was measured in the centre of the field plots with a SPAD-502 chlorophyll meter (Minolta, Valencia, Spain). The unitless SPAD-502 values are only useful if a proper statistical relationship with leaf chlorophyll has initially been established. Thus, 55 leaf samples representing the phenological range from tillering to anthesis were randomly selected from the green leaf fraction of the destructive samples. These samples were then thoroughly measured with the SPAD-502, with a measurement for every 1- to 2-cm leaf in the sample. The leaf samples were subsequently cut into 1- to 2-cm square pieces, frozen, and later analyzed for chlorophylls *a* and *b* in the laboratory.

2.2.2. Organic extraction of leaf chlorophyll

Chlorophyll was extracted using the common *N*,*N*-dimethylformamide solvent method (Inskeep & Bloom, 1985; Moran, 1992; Moran & Porath, 1980). This solvent facilitates extraction of the chlorophylls without maceration of the leaf tissue. Extinction coefficients published by Porra, Thompson, and Kriedemann (1989) for chlorophyll pigments diluted in *N*,*N*-dimethylformamide were used to calculate the concentrations. The results represent four

determinations based on duplicate analyses of each of the two field samples.

2.2.3. Relating SPAD-502 measurements to LCC

Although some authors have found linear relationships between SPAD values and LCC (Adamsen et al., 1999; Campbell, Mobley, Marini, & Pfeiffer, 1990; Schaper & Chacko, 1991; Yadava, 1986), others have found a curvilinear relationship to apply (Manetas, Grammatikopoulus, & Kyparissis, 1998; Markwell, Ostermann, & Mitchell, 1995; Monje & Bugbee, 1992). In-depth discussions of the relationship between SPAD values and leaf chlorophyll concentrations are rarely found in the literature. However, Markwell et al. (1995) present theoretical justification for using an exponential equation to describe the relationship between LCC and the SPAD-502 meter output value.

Thorough inspection of our data suggested that the SPAD-502–chlorophyll relationship also is affected by leaf density, which is related to the age of the leaf. We used the specific leaf area index (SLA) as an indicator of green leaf dry matter density. SLA is defined as the ratio of AGL to green leaf dry matter by weight (cm^2/mg). A multivariate linear regression analysis was applied to the data with LCC and 1/SLA including their products and crossproduct as independent variables. This analysis proved that both LCC and 1/SLA were significant predictors at the 95% confidence level. Thus, both of these variables were included in the model. However, neither the products nor the crossproducts of these variables were significant, suggesting that the remaining variance may be attributed to experimental errors. Analyses of the residuals suggested a logarithmic transformation of the chlorophyll data, supporting the arguments in favour of an exponential relationship between leaf chlorophyll and SPAD-502 readings. The resulting curvilinear model then reads (Eq. (2)):

$$\mathrm{LCC}\ (\mathrm{mg/m^2}) = \exp^{(0.04245\mathrm{SPAD}+0.05685/\mathrm{SLA}+4.138)} \qquad (r^2 = .90) \qquad (2)$$

Thus, this function was used to convert SPAD-502 values obtained in the field to LCC.

2.3. CCD

The SPAD-502 measurements were performed weekly between May 21, 1997 and June 29, 1997 in conjunction with nondestructive measurements of leaf area index (LAI) obtained with a LAI-2000 Canopy Analyzer (LI-COR). This instrument uses radiation measurements made above and within the canopy to determine canopy light interception at five angles from which the canopy area index (CAI) and leaf mean tip angle (MTA) can be computed from a radiative transfer model (Welles & Norman, 1991).

CCD can be considered as a measure of the potential photosynthetic capacity (Blackburn, 1998). It is calculated based on GCAI and vertical profile measurements of LCC and CAI. The CAI slices were determined from LAI-2000 profile measurements acquired with 10-cm increments. The CAI values derived from LAI-2000 measurements acquired before heading were significantly lower than the GCAI values calculated based on the destructive measurements. For that reason, the LAI-2000-based CAI measurements were used only to determine the vertical foliage density distribution. This distribution was used to assign weights to the LCCs associated with each vertical slice (i) of the canopy. The average LCC ($\overline{\mathrm{LCC}}$) in the vertical profile was thus calculated as (Eq. (3)):

$$\overline{\mathrm{LCC}}\ (\mathrm{mg/m^2}) = \sum_{i=1}^{i=n} \mathrm{LCC}_i \left(\frac{\mathrm{CAI}_{(i-1)} - \mathrm{CAI}_i}{\mathrm{CAI}_0} \right) \qquad (3)$$

and CCD was calculated as the product of GCAI and $\overline{\mathrm{LCC}}$ (Eq. (4)):

$$\mathrm{CCD}\ (\mathrm{mg/m^2}) = \mathrm{GCAI} \times \overline{\mathrm{LCC}} \qquad (4)$$

2.4. Spectral reflectance measurements

A GER-2600 spectrometer (GER, Millbrook, NY, USA) was used to measure the spectral radiance in the field. The spectrometer was equipped with a 10° field of view fore optic and operated from a hydraulic lift 6.25 m above the ground. This corresponds to a sensor footprint of 0.94 m^2. All measurements were obtained at nadir and within ±2 h of local solar noon. The reflected radiances were converted to spectral reflectance by normalization with radiances measured over a white Spectralon reflectance standard (Spectralon; Labsphere, North Sutton, NH, USA). The spectra were further corrected for non-Lambertian properties of the Spectralon material using the calibration equations given by Jackson, Clarke, and Moran (1992). The spectral resolution of the GER-2600 is roughly 2.5 nm in the visible (vis) and NIR region. Sixteen scans were averaged for every measurement and, in most cases, 30 measurements were obtained and averaged over each field plot. Reference measurements of the Spectralon were obtained for every five canopy spectral measurements. The corrected spectra were spectrally resampled to a bandwidth of 10 nm using a cubic spline function (Press, Flannery, Teukolsky, & Vetterling, 1989). Although this resampling method may not work well for all spectral reflectance data sets, we found that the absolute discrepancy between reflectance values of resampled vegetation spectra and averaged measured values was less than 0.02%.

3. Calculation of VIs

Pinter, Jackson, Ezra, and Gausman (1985) showed that the spectral reflectance of vegetation depends on canopy

Table 2
VI formulae

Acronym	Name	VI	Reference
RVI	Ratio vegetation index	$\mathrm{RVI} = \frac{\rho_{\mathrm{NIR}}}{\rho_{\mathrm{Red}}}$	(Pearson & Miller, 1972)
NDVI	Normalized difference vegetation index	$\mathrm{NDVI} = \frac{\rho_{\mathrm{NIR}} - \rho_{\mathrm{Red}}}{\rho_{\mathrm{NIR}} + \rho_{\mathrm{Red}}} = \frac{\mathrm{RVI} - 1}{\mathrm{RVI} + 1}$	(Rouse, Haas, Schell, Deering, & Harlan, 1974)
PVI	Perpendicular vegetation index	$\mathrm{PVI} = \frac{\rho_{\mathrm{NIR}} - a\rho_{\mathrm{Red}} - b}{\sqrt{1 + a^2}}$	(Richardson & Wiegand, 1977)
DVI	Difference vegetation index	$\mathrm{DVI} = \rho_{\mathrm{NIR}} - \rho_{\mathrm{Red}}$	(Jordan, 1969)
TSAVI	Transformed soil-adjusted vegetation index	$\mathrm{TSAVI} = \frac{a(\rho_{\mathrm{NIR}} - a\rho_{\mathrm{Red}} - b)}{a\rho_{\mathrm{NIR}} + \rho_{\mathrm{Red}} - ab}$	(Baret, Guyot, & Major, 1989)
ATSAVI[a]	Adjusted transformed soil adjusted vegetation index	$\mathrm{ATSAVI} = \frac{a(-a\rho_{\mathrm{Red}} - b)}{a\rho_{\mathrm{NIR}} + \rho_{\mathrm{Red}} - ab + X(1 + a^2)}$	(Baret & Guyot, 1991)
SAVI2	Second soil-adjusted vegetation index	$\mathrm{SAVI2} = \frac{\rho_{\mathrm{NIR}}}{\rho_{\mathrm{Red}} + b/a}$	(Major et al., 1990)
MSAVI2	Modified second soil-adjusted vegetation index	$\mathrm{MSAVI2} = \frac{1}{2}\left[2(\rho_{\mathrm{NIR}} + 1) - \sqrt{(2\rho_{\mathrm{NIR}} + 1)^2 - 8(\rho_{\mathrm{NIR}} - \rho_{\mathrm{Red}})}\right]$	(Qi, Chehbouni, Huete, Kerr, & Sorooshian, 1994)
RDVI	Renormalized difference vegetation index	$\mathrm{RDVI} = \sqrt{\mathrm{NDVI} \times \mathrm{DVI}}$	(Reujean & Breon, 1995)
CARI	Chlorophyll absorption ratio index	$\mathrm{CARI} = \frac{\lvert(a \times 670 + \rho_{670} + b)\rvert}{\sqrt{(a^2 + 1)}} \frac{\rho_{700}}{\rho_{670}}$ $a = (\rho_{700} - \rho_{550})/150, \quad b = \rho_{550} - (a \times 550)$	(Kim et al., 1994)
R750/R700	R750/R700	$\frac{\rho_{750}}{\rho_{700}}$	(Gitelson & Merzlyak, 1996)
R750/R550	R750/R550	$\frac{\rho_{750}}{\rho_{550}}$	(Gitelson & Merzlyak, 1996)
TVI	Triangular vegetation index	$\mathrm{TVI} = 60(\rho_{\mathrm{NIR}} - \rho_{\mathrm{Green}}) - 100(\rho_{\mathrm{Red}} - \rho_{\mathrm{Green}})$	(Broge & Leblanc, 2001)
REIP_Gaus[b]	Red edge inflection point (Gaussian model)	$R(\lambda) = R_s - (R_s - R_0)\exp\left(\frac{-(\lambda_0 - \lambda)^2}{2\sigma^2}\right)$ $\mathrm{REIP\_Gaus} = \lambda_i + \sigma$	(Miller et al., 1990) (Broge & Leblanc, 2001)
REIP_Poly[c]	Red edge inflection point (polynomial model)	$R(\lambda) = c_0 + c_1\lambda + c_2\lambda + c_3\lambda + c_4\lambda + c_5\lambda + c_6\lambda$ REIP_Poly = root of the second derivative ($R''(\lambda) = 0$), where λ is closer to 720 nm	(Broge & Leblanc, 2001)
REIP_Lagr[d]	Red edge inflection point (Lagrangian model)	$\mathrm{REIP\_Lagr} = \frac{A(\lambda_i + \lambda_{i+1}) + B(\lambda_{i-1} + \lambda_{i+1}) + C(\lambda_{i-1} + \lambda_i)}{2(A + B + C)}$ $A = \frac{D_{\lambda(i-1)}}{(\lambda_{i-1} - \lambda_i)(\lambda_{i-1} - \lambda_{i+1})}$ $B = \frac{D_{\lambda(i)}}{(\lambda_i - \lambda_{i-1})(\lambda_i - \lambda_{i+1})}$ $C = \frac{D_{\lambda(i+1)}}{(\lambda_{i+1} - \lambda_{i-1})(\lambda_{i+1} - \lambda_i)}$	(Dawson & Curran, 1998)

(continued on next page)

Table 2 (*continued*)

1DZ_DGVI[e]	First-order derivative green vegetation index (zero baseline)	$1DZ\_DGVI = \sum_{\lambda_i}^{\lambda_n} \lvert\rho'(\lambda_i)\rvert \Delta\lambda_i$	(Elvidge & Chen, 1995)
2DZ_DGVI[e]	Second-order derivative green vegetation index (zero baseline)	$2DZ\_DGVI = \sum_{\lambda_i}^{\lambda_n} \lvert\rho''(\lambda_i)\rvert \Delta\lambda_i$	(Elvidge & Chen, 1995)
CACI[f]	Chlorophyll absorption continuum index	$CACI = \sum_{\lambda_i}^{\lambda_n} (\rho_i^c - \rho_i)\Delta\lambda_i, \quad \rho_i^c = \rho_i + i\frac{d\rho^c}{d\lambda}\Delta\lambda_i$	(Broge & Leblanc, 2001)
CRCAI	Continuum-removed chlorophyll absorption index	$CRCAI = \sum_{\lambda_i}^{\lambda_n} \frac{\rho_i^c - \rho_i}{\rho_i^c}\Delta\lambda_i, \quad \rho_i^c = \rho_i + i\frac{d\rho^c}{d\lambda}\Delta\lambda_i$	(Broge & Leblanc, 2001)
CRCWD	Continuum-removed chlorophyll well depth	$CRCAI = 1 - \rho_{670}^c$	(Broge & Leblanc, 2001)

ρ denotes reflectance, λ denzotes wavelength, and *a* and *b* are the soil line coefficients.

[a] *X* is an adjustment factor, which is set to minimize background effects (*X*=0.08 in the original paper).

[b] R_s is the "shoulder" spectral reflectance, R_0 is the minimum spectral reflectance at wavelength λ_0 corresponding to the chlorophyll absorption well. λ is wavelength, and σ is the Gaussian function deviation parameter.

[c] $c_0, c_1, \ldots, c_6$ are the coefficients associated with the polynomial fit in reflectance space.

[d] $D_{\lambda(i)}$ is the first derivative value of the band *i* with the maximum first derivative. $D_{\lambda(i-1)}$ and $D_{\lambda(i+1)}$ are the first derivative values of adjacent bands.

[e] Δλ denotes the band width.

[f] ρ^c is the reflectance continuum.

architecture, where planophile canopies tend to exhibit higher reflectance in the vis–NIR range than erectophile ones. They also showed that the reflectance of erectophile canopies is more sensitive to the solar zenith angle than the reflectance of planophile canopies with similar biophysical characteristics. Soil evaporation tends to be higher in open than in closed canopies. As a consequence, the soil surface dries out faster when the mean leaf inclination angle is increasing for the same foliage area. Soil surface drying is associated with increasing spectral reflectance (Irons, Weismiller, & Petersen, 1989).

To reduce such effects, reflectance data can be translated into a VI (Moulin & Guérif, 1999), usually calculated from the red and NIR band. Numerous VIs have been developed to characterize vegetation canopies. They generally attempt to enhance spectral reflectance of green plant fractions while trying to minimize the spectral effects caused by variations in soil color, irradiance conditions, sun angle, amount of senescent vegetation, and atmospheric composition. A detailed discussion on VI theory can be found in Huete (1989). Many of the VI formulations presented in the following encompass the red band (650 nm) and/or the NIR band (800 nm), but some also include a green band (550 nm). When reflectances measured in other bands are used in the formulation of a VI, the band centre wavelength is provided as a subscript (in nanometers). The VI formulae and notable references are provided in Table 2. Broad-band indices were calculated by spectral resampling of the 10-nm data using the Landsat TM5 filter functions.

The early VIs are generally divided into *ratio* indices and *orthogonal* indices. Ratio-based VIs are often preferred over orthogonal-based VIs because the soil spectral characteristics needed to establish a soil line in the red–NIR space often are unavailable or influenced by soil variability. The soil line is defined by the coefficients *a* and *b* giving the slope and intercept as determined by linear regression of the soil reflectance in the red–NIR spectral space (Richardson & Wiegand, 1977). For our purpose, a soil line based on five series of soil spectra was established (Table 3). The soil spectra were collected on different dates throughout the growing season and represent the full range of soil surface moisture regimes encountered under natural conditions. The selected early VIs, RVI, NDVI, PVI, DVI, TSAVI, ATSAVI, SAVI2, MSAVI2, and RDVI are all based on discrete red and NIR bands. Kim, Daughtry, Chappelle, and McMurtrey (1994) found the ratio of ρ_{550} and ρ_{700} to be constant at the leaf level, regardless of differences in chlorophyll concentrations, and defined a chlorophyll absorption ratio index (CARI) based on this property. Gitelson, Merzlyak, and Lichtenthaler (1996) and Lichtenthaler, Gitelson, and Lang (1996) explored this idea and found strong correlation between LCC and the reflectance ratios ρ_{750}/ρ_{700} and ρ_{750}/ρ_{550}. Broge and Leblanc (2001) introduced the triangular vegetation index (TVI),

Table 3
Soil line coefficients derived from soil spectral measurements based on spectral measurements at 650 and 800 nm, as well as spectral measurements resampled to match the band configuration of Landsat 5 using the TM spectral response function

Equation	*a*	*b*	DOF	R^2	S.E. (*b*)	S.E. (*a*)
R800 = *a* × R650 + *b*	1.39	1.938	308	.9822	0.1234	0.01069
TM4 = *a* × TM3 + *b*	1.427	2.295	308	.9826	0.1291	0.01083

Soil type is Dystic Luvisol (ISSS Working Group RB, 1998).

which is a function of the difference between red and NIR reflectance and the magnitude of green reflectance. It is defined as the area spanned by a triangle floating in spectral reflectance space.

In recent years, emphasis has been on the development of more sophisticated ways of interpreting spectral signatures, some of which are based on waveform analysis techniques.

The characteristic red edge reflectance pattern of vegetation has been the subject of many studies (Blackburn, 1998; Collins, 1978; Gilabert, Gandia, & Melia, 1996; Gitelson et al., 1996; Horler, Dockray, & Barber, 1983; Pinar & Curran, 1996), all of which have shown the observed blue- and red shift of the red edge inflexion point (REIP) to be related to plant growth conditions. REIP can be defined as the wavelength where the first derivative of the spectral reflectance is maximum. REIP shifts toward shorter wavelengths (blue shift) are associated with a decrease in green vegetation density, just as REIP shifts toward longer wavelengths (red shift) are associated with an increase in green plant material. In the present study, five different methods were applied to parameterize the REIP spectral shift, including two measures that depend on the shape of the red edge.

Miller, Hare, and Wu (1990) used an inverted Gaussian model to describe the variation of reflectance as a function of wavelength, $R(\lambda)$, and thereby determine REIP. This approach has the advantage that it has a built-in smoothing of the red edge reflectance values and has been used by several authors (Bonham-Carter, 1988; Broge, Hvidberg, Hansen, Andersen, & Nielsen, 1997). A similar way of determining REIP is by fitting a higher-order polynomial to the reflectance data in the red edge spectral range. A high-order polynomial is capable of capturing the asymmetry, if any, of the spectral reflectance across the red edge, whereas such asymmetry will be averaged out by the inverted Gaussian model. In this study, a sixth-order polynomial was applied to parameterize $R(\lambda)$. REIP was then determined by identifying the roots of the second derivative of the polynomial ($R''(\lambda)=0$), adopting the root where λ was closer to 720 nm.

Recently, Dawson and Curran (1998) proposed a new way of determining REIP. They applied a technique known as Lagrangian interpolation, which is applied to the first-derivative transformation of the reflectance spectrum. The technique fits a second-order polynomial curve to three bands, from which the REIP is determined. This approach was adopted as the third and last method of determining the REIP of the narrow-band data.

Elvidge and Chen (1995) calculated the first and second derivatives of the spectral reflectance data and integrated the absolute derivative values over the spectral region from 626 to 795 nm. They denoted these indices 1DZ_DGVI and 2DZ_DGVI. They also integrated the first derivative spectra with respect to the local baseline (1DL_DGVI). The performances of the latter two indices were shown to be practically identical and thus only 1DZ_DGVI and 2DZ_DGVI were considered in this study.

An alternative way of utilizing hyperspectral reflectance data is to calculate the spectral continuum (Clark & Roush, 1984) in which the analysis is based on the shape or area of the troughs spanned by the spectral continuum. Broge and Leblanc (2001) defined the chlorophyll absorption continuum index (CACI) as the area spanned by the chlorophyll absorption continuum ($\sim$550 to $\sim$730 nm) and the spectral reflectance curve. This index is similar to the TVI index in the sense that both indices represent the area spanned by the spectral reflectance between the green peak and the NIR shoulder.

Continuum removal is taking this approach one step further. Continuum removal is a means of normalizing reflectance spectra to allow for direct comparison of individual absorption features from a common baseline (Clark & Roush, 1984). This approach is mostly used by geologists looking for distinct narrow absorption features in the spectra, i.e., physical fingerprints of minerals (Kruse, 1988). However, the technique can be used to identify and quantify any material that exhibits a discrete absorption feature such as chlorophylls in live vegetation. Broge and Leblanc (2001) introduced the continuum-removed chlorophyll absorption index (CRCAI), defined as the area spanned by the continuum-removed spectra and the continuum, i.e., the $y=1$ line after continuum removal. Another measure of the continuum-normalized spectrum is the maximum depth of the chlorophyll absorption trough (Broge & Leblanc, 2001). This measure, the continuum-removed chlorophyll well depth (CRCWD), has a value between 0 and 1. It is thus directly comparable with many traditional VIs such as NDVI and TSAVI.

4. Relating GCAI and CCD to the VIs

It was not always possible to acquire spectral measurements at the same moment at which the biophysical data were collected. In some cases, these measurements were even obtained 3–4 days apart. Thus, an interpolation procedure was required. We chose curve-fitting techniques based on day of year (DOY) to calculate the missing GCAI and LCC values. This procedure has a built-in smoothing effect, which helps minimize experimental errors. However, it also tends to filter out subtle variations in plant development. A y-transformed third-order polynomial provided the best fit to the GCAI data (Eq. (5)), whereas a two-term polynomial provided the best fit for the LCC data (Eq. (6)):

$$\mathrm{GCAI} = \sqrt{a + b\mathrm{DOY} + c\mathrm{DOY}^2 + d\mathrm{DOY}^3} \tag{5}$$

$$\mathrm{LCC} = \alpha + \beta\mathrm{DOY}^{2.5} + \frac{\gamma}{\mathrm{DOY}^2} \tag{6}$$

The coefficients for the curve fits are listed in Table 4a and b together with some basic statistics.

Table 4

Coefficients/statistics	W40N	W80N	W120N
(a) Coefficients of curve fit to GCAI measurements (Eq. (5)). The data were acquired between May 2 and July 7, 1997 (DOY 122–DOY 188)			
Observations	11	11	11
a	-2.6917×10^{-3}	-3.1581×10^{-3}	-3.2601×10^{-3}
b	-1.3465×10^{-1}	-1.5991×10^{-1}	-1.6628×10^{-1}
c	1.9446×10^{-3}	2.2669×10^{-3}	2.3713×10^{-3}
d	-6.5012×10^{-6}	-7.4517×10^{-6}	-7.8133×10^{-6}
Min. GCAI (−)	0.07	0.27	0.74
Max. GCAI (−)	2.79	4.25	5.04
r^2	.9539	.9436	.9264
S.E. of fit	0.2437	0.3619	0.4849
(b) Coefficients of curve fit to LCC measurements (Eq. (6)). The data were acquired between May 20 and June 30, 1997 (DOY 141–DOY 181)			
Observations	11	11	11
α	−47.995	−188.18	−187.7
β	1.0050×10^{-4}	3.1608×10^{-4}	3.1538×10^{-4}
γ	1.1353×10^{6}	3.1360×10^{6}	3.2825×10^{6}
Min. LCC ($\mu g/cm^2$)	26.2	34.5	40.4
Max. LCC ($\mu g/cm^2$)	33.9	50.8	58.8
r^2	.24	.531	.4874
S.E. of fit	2.3384	3.2577	3.4984

Most VIs, including the REIP, exhibit decreasing sensitivity followed by saturation with increasing greenness. However, some VIs, such as RVI, tend to be almost linearly related to canopy greenness. This study investigates the relationships using a simple linear model, as well as a more flexible exponential model suggested by Baret and Guyot (1991) and Wiegand et al. (1992). The latter is a modified version of Beer's Law expressing the variation of a VI as a function of the greenness measure G (Eq. (7)).

$$\mathrm{VI} = \mathrm{VI}_\infty + (\mathrm{VI}_g - \mathrm{VI}_\infty)\exp^{K_{\mathrm{VI}}G} \tag{7}$$

It assumes a homogenous canopy with an optical thickness given by G. The dynamic range of the VI is expressed as the difference between the bulk vegetation index, VI_∞, and the index value corresponding to bare soil conditions, VI_g. The K_{VI} parameter is equivalent to the extinction coefficient in Beer's Law and represents the relative increase in VI due to an elementary increase in G. Wiegand et al. (1992) compared this model (Eq. (7)) with power and exponential transformations and found that it was the best to relate VIs to biophysical parameters. Thus, it was adopted herein to express the relationship between the calculated VIs and GCAI and CCD.

The RMSE and the adjusted coefficient of determination (R^2) were calculated along with the normalized RMSE (NRMSE) given as $\mathrm{RMSE}/(\mathrm{VI}_{\mathrm{Max}} - \mathrm{VI}_{\mathrm{Min}})$, where $\mathrm{VI}_{\mathrm{Max}}$ and $\mathrm{VI}_{\mathrm{Min}}$ refer to the minimum and maximum values of the VI. These values are calculated from the minimum and maximum biophysical parameters in the data set using the fitted model.

The calculated statistics (R^2, RMSE, and NRMSE) are all associated with the accuracy of the curve fit, but they do not provide any information about the prediction power of the VIs because of the nonlinear nature of the relationship between the VIs and the biophysical parameters. The prediction power is inversely related to the sensitivity to all parameters other than the greenness measure G (in this study, GCAI or CCD) for which the VI serves as a predictor. To obtain this information, the shape of the exponential function relating the VIs and the biophysical parameters needs to be considered in conjunction with the associated variance. This was achieved using the concept of relative equivalent noise (REN) introduced by Baret and Guyot (1991), which effectively is the standard error of the VI at a given value of the biophysical parameter. In the REN approach, the local slope of the exponential function fitted to the data is used to calculate the standard deviation of the greenness estimate according to the equation (Eq. (8)):

$$\mathrm{REN}_G = \frac{\sigma_G}{G} = \frac{\sigma_{\mathrm{VI}}}{G}\left(\frac{\mathrm{d}(\mathrm{VI})}{\mathrm{d}(G)}\right)^{-1} \tag{8}$$

The local slope can be found by differentiation of Eq. (7):

$$\frac{\mathrm{d}(\mathrm{VI})}{\mathrm{d}(G)} = -K_{\mathrm{VI}}(\mathrm{VI}_g - \mathrm{VI}_\infty)\exp^{(-K_{\mathrm{VI}}G)} \tag{9}$$

The advantage of the REN measure is that it allows for a comparison of VIs for any value or interval of values of the independent variable (GCAI or CCD), thus facilitating a unique method for comparing the performance of different VIs. For the estimation of CGAI, the best-fitting results were obtained when restraints were applied to the estimation of VI_∞. This is consistent with the results of Broge and Leblanc (2001).

The R^2 statistic is defined as the proportion of variance of the response that can be explained by the regressor variable(s). However, the R^2 statistic can be misleading when comparing results of experiments on the same variable but with different ranges for the regressors, such as the experi-

ment reported herein. In such cases, one should look at the standard error of prediction (root mean square error) rather than at R^2 (SAS Institute, 1988). For these reasons, we decided to base the comparison of the VIs on the NRMSE and REN.

5. Results and discussion

Destructive sampling showed that stems can represent up to 25% of the total green area of a winter wheat crop prior to heading (Fig. 1). This percentage increases during senescence when GLAI is reduced due to leaf chlorosis. Because the LAI-2000 measurements do not allow for segregation of leaf area and area of other plant constituents, the calculated values of LCC were assumed to apply to all green plant fractions. This may be a reasonable assumption for the growth stages prior to elongation, where leaves embrace the stem (Zadoks, Chang, & Konzak, 1974), but the technique needs to be validated for the growth stages succeeding elongation. Further, the calculation of postheading GCAI and CCD values builds on the assumption that senescence in stems and ears proceeds at the same rate as in leaves.

Our data set clearly shows that canopy spectral reflectance is influenced by the soil background. Especially, the plot with the least available plant N (W40N) exhibits large variations in red reflectance during the growth season. The W40N plot is characterized by a lower GLAI and a more erectophile appearance due to N deficiency, both of which cause more exposure of the soil background. Fig. 2b and c shows the typical red and NIR response for each of the plots reflecting the seasonal pattern of wheat canopy green up followed by senescence. Closer inspection reveals that all peaks in red reflectance appear at times where:

1. No major rainfall events have occurred during the previous day, thus allowing the soil crust to dry and brighten before measurements.
2. Solar zenith angles are relatively small, causing an increase of the fraction of directly illuminated soil.

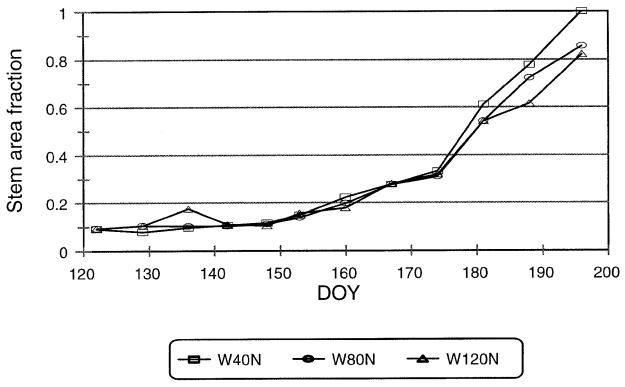

Fig. 1. Total stem area fraction relative to total area of all green plant fragments. Maximum GCAI in all plots was measured at DOY 160.

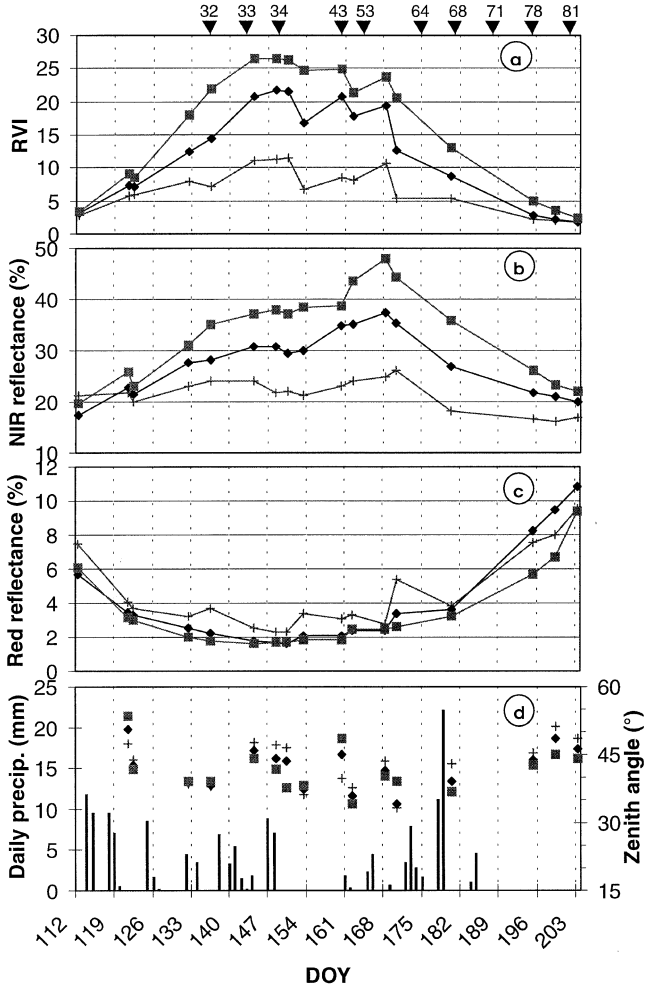

Fig. 2. Seasonal change of RVI (a) and reflectance factors of red (b) and NIR (c). Data are means of 30 observations per treatment, where each observation represents an average of 16 measurements. The treatments represent three levels of N fertilisation: 40 kg N/ha (+); 80 kg N/ha (◆); 120 kg N/ha (■). The crop phenological development is indicated in (a) as Zadoks' numbers (Zadoks et al., 1974). The amount of daily precipitation and the solar zenith angle at the time of observation are also indicated (d).

Similar observations were made by Hinzman et al. (1986), and it seems reasonable to assume that the variation observed, especially in red reflectance, can be attributed to the combined effects of variations in background reflectance and changes in background exposure. This has significant implications for some of the VIs, e.g., RVI that has red reflectance as the index denominator (Table 2). Fig. 2a shows the seasonal variation of RVI. The dips in the temporal RVI curve correspond to the peaks in the red reflectance curve observed at DOY 137, 153, 160, 163, and 170.

The first step in the analysis of the VIs was to compare the exponential model with the linear model for each of the VIs based on the NRMSE values. The exponential model gave lower NRMSEs than the linear model for all indices

except for the narrow-band version of RVI. The differences in NRMSE between the linear and exponential RVI–GCAI and RVI–CCD relationships were both very small (Fig. 3), suggesting that RVI is linearly related to GCAI and CCD. This is consistent with other results from the literature (Goel, 1989; Hinzman et al., 1986; Thomsen, Schelde, Heidmann, & Hougaard, 1997).

In the second step of the analysis, the broad-band satellite-based VIs were compared to their narrow-band counterparts to see if narrow bands positioned directly on the chlorophyll absorption band and well onto the NIR shoulder would improve the prediction accuracy. The analysis of the GCAI–VI exponential relationships showed that the narrow-band VIs were no better than their broad-band counterparts at predicting GCAI. The difference in terms of

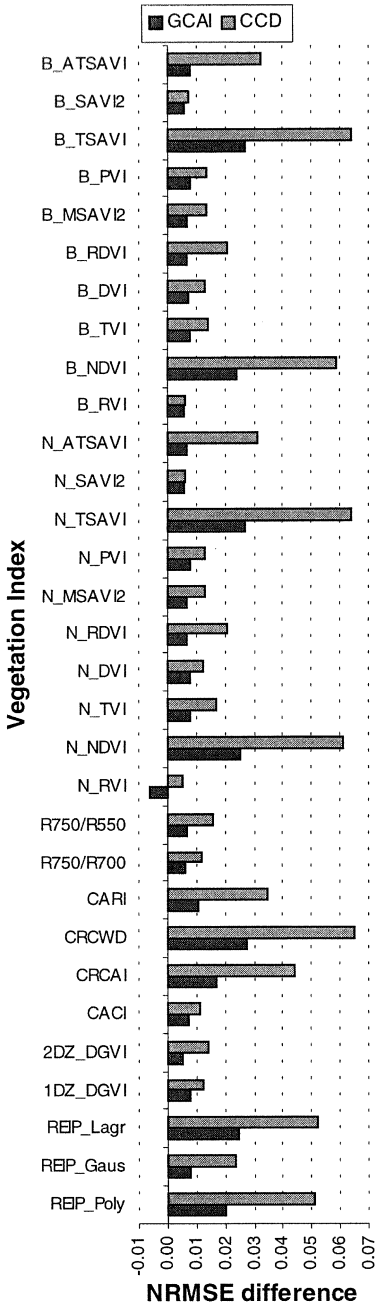

Fig. 3. The difference in NRMSE between the linear and the exponential model (Eq. (7)). Positive values indicate that the exponential model gives a better fit to the data.

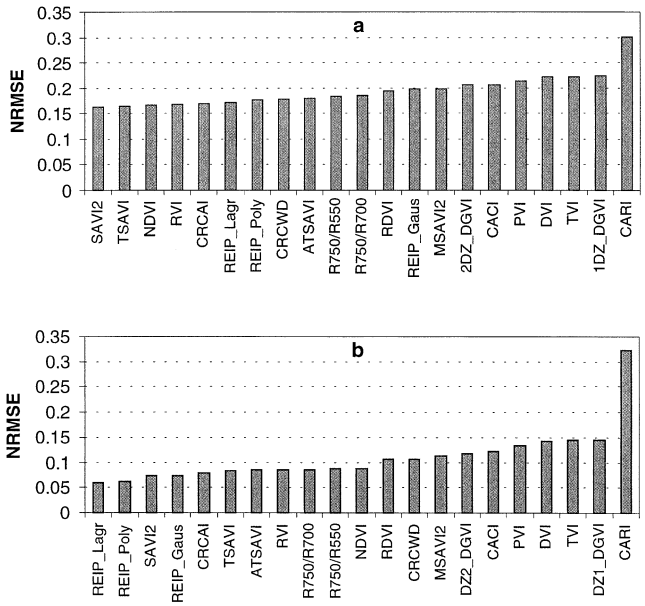

Fig. 4. NRMSE of the relationship between the VIs and greenness expressed as GCAI (a) and CCD (b).

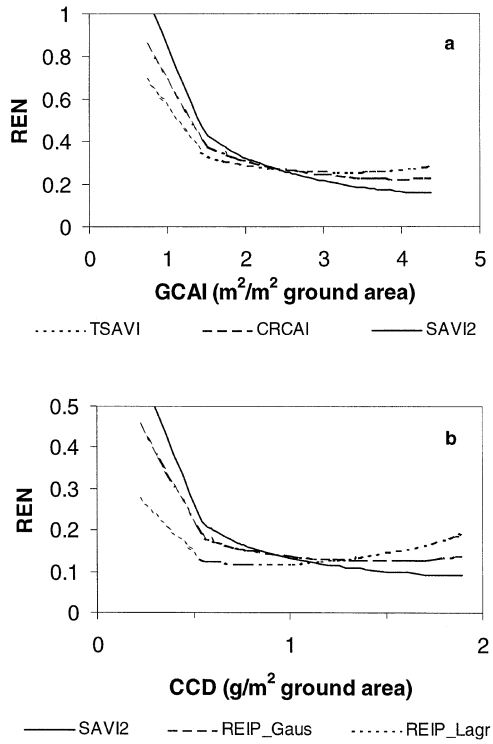

Fig. 5. Relative equivalent noise for the best three indices calculated as a function of greenness expressed in terms of GCAI (a) and CCD (b).

NRMSE was less than 5% for all indices. The same was found for the CCD–VI linear relationships with the exception of NDVI, TSAVI, and SAVI2 that proved slightly more accurate with NRMSE differences of 11%, 15%, and 7%, favouring the broad-band versions of these indices. These results are consistent with the results presented by Broge and Leblanc (2001), who tested the GLAI and CCD prediction ability of the same range of indices based on simulated data. On this basis, we chose to use the broad-band VIs in the subsequent analysis.

In the third and final step of the analysis, the best indices for predicting GCAI and CCD were identified from their NRMSE values. Further, the dynamic nature of the VIs was investigated using the REN concept. The results indicate that GCAI estimation accuracy is much less dependent on the choice of VI than is the CCD estimation accuracy in terms of NRMSE (Fig. 4). Excluding the CARI, which did not perform well at all, the relative accuracy associated with GCAI prediction varies by no more than 40% between the various VIs, whereas the relative accuracy associated with CCD prediction varies by more than 120%.

The SAVI2 index proposed by Major, Baret, and Guyot (1990) seems to be the best overall choice as an estimator of CGAI. However, the hyperspectral indices based on the REIP (REIP_Lagr and REIP_Poly) seem to be the best overall predictors of CCD, closely followed by the SAVI2 index. Again, these results are in agreement with the simulation study by Broge and Leblanc (2001).

The dynamics of each VI can be expressed by the REN associated with the relationship between the VI and the biophysical parameter. The REN values for all indices were plotted as a function of GCAI and CCD. The indices that are the best predictors within the range or part of the range of the biophysical parameter can be identified as the ones on the lower boundary of the space spanned by the graphs. Fig. 5 presents the REN values for the best of the predictors. Fig. 6 presents the associated best-fit curves based on Eq. (7) for these predictors. The NRMSE value associated with the exponential relation between SAVI2 and GCAI (Fig. 5b) is only marginally lower than the NRMSE value associated with the linear relation derived by simple linear regression analysis. Observations representing complete canopy closure, i.e., GCAIs around 10 or higher, are needed in order to reach the point of saturation of the SAVI2, thus enabling a true value of VI_{∞} to be defined. With the current data set, the modelled VI_{∞} for SAVI2 approaches the upper boundary limit that was set to 800 while K_{VI} approaches zero.

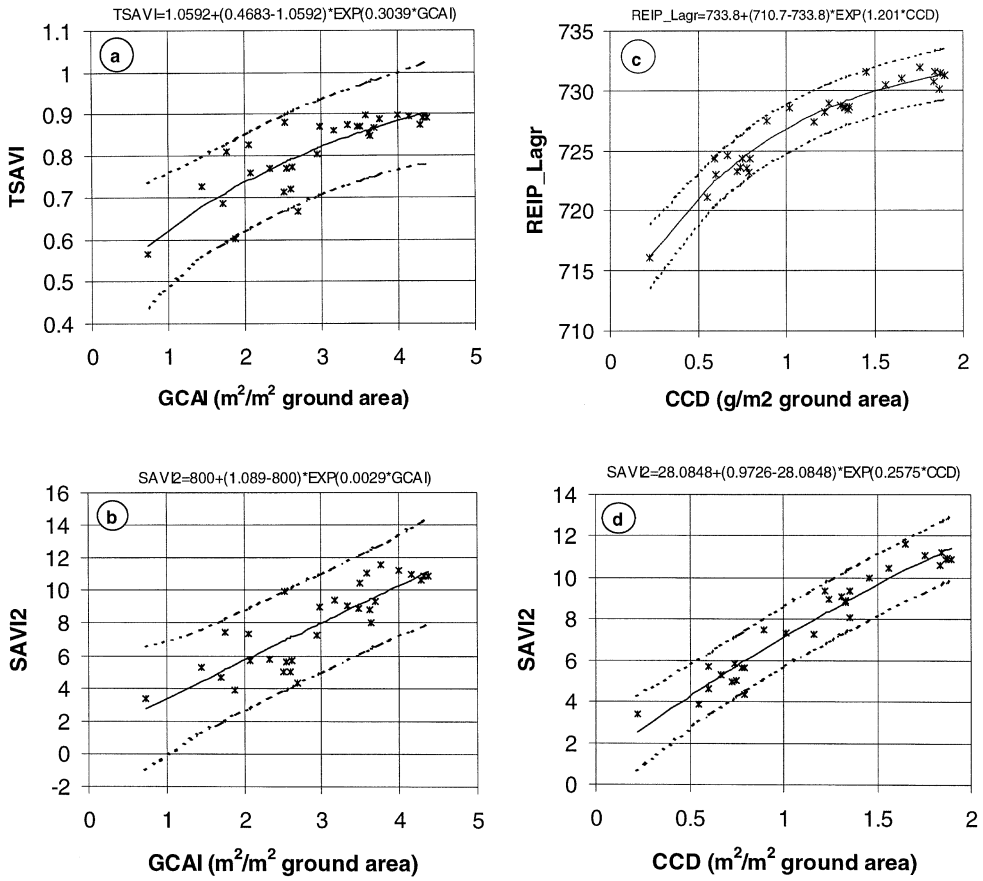

Fig. 6. Curve fits (solid line) and 95% confidence limits (broken lines) of the best predictors. The curve fits are based on the exponential model (Eq. (7)) and represent the best predictors of GCAI (a,b) and CCD (c,d).

6. Conclusion

The relationship among all VIs and the greenness parameter (GCAI or CCD) was best described by an exponential function, except for the narrow-band RVI relationship with GCAI.

The narrow-band versions of the traditional indices including the TVI were not better predictors of GCAI than their broad-band counterparts. Normalized root mean squares differed by less than 5% in favour of the broad-band indices. However, the accuracy of CCD prediction increased by up to 15% when broad-band VIs were chosen.

Generally, CCD can be estimated with a higher degree of accuracy than can GCAI. However, the choice of VI is of greater importance when estimating CCD. Thus, besides the CARI, the relative accuracy of GCAI estimation varies by no more than 40% with the choice of VI. In comparison, the relative accuracy of CCD estimation may vary by more than 120% with the choice of VI.

The REN concept was used to analyze the dynamics of each VI as a predictor of GCAI and CCD. For wheat canopies with GCAI < 2, the TSAVI proved to be the best predictor, whereas SAVI2 was the best when GCAI > 2. The best predictors of CCD were REIP_Lagr (CCD < 1 g/m^2 ground area) and SAVI2 (CCD > 1 g/m^2 ground area).

While the hyperspectral indices were not superior to predict GCAI, they generally behaved better with CCD. SAVI2 is the best candidate for an all-round index because it is a good predictor of both variables. Further, SAVI2 has been proven to be relatively insensitive to external parameters such as background reflectance and atmospheric effects (Broge & Leblanc, 2001).

The results presented in this study are in agreement with those of a recent study based on simulated data (Broge & Leblanc, 2001) considering a wide range of canopy conditions. This suggests that they may also apply to other monocultures. However, a more extensive database containing data from different locations and years is required in order to strengthen the relationships between the VIs and the greenness measures.

Future studies should employ a spectral resampling routine that represents the reflectance as an average value calculated over the full width of each new band. Simple linear interpolation between spectral reflectances combined with band aggregation may be the most feasible way of spectral resampling. Further, the assumption, that senescence in stems and ears proceeds at the same rate as in the leaves, should be avoided.

Acknowledgments

This work was carried out as part of the Danish Multisensor Airborne Campaign (DANMAC) project funded by the Danish Research Councils. The authors are indebted to Henning Jensen (Hydro Agri Denmark) and Jörgen Wolring (Hydro Agri Germany) for kindly lending out one of their Minolta SPAD-502 chlorophyll meters.

References

Adamsen, F. J., Pinter Jr., P. J. , Barnes, E. M., LaMorte, R. L., Wall, G. W., Leavitt, S. W., & Kimball, A. (1999). Measuring wheat senescence with a digital camera. *Crop Science*, *39*, 719–724.

Baret, F., & Guyot, G. (1991). Potentials and limits of vegetation indices for LAI and APAR assessment. *Remote Sensing of Environment*, *35*, 161–173.

Baret, F., Guyot, G., & Major, D. J. (1989). TSAVI: a vegetation index which minimizes soil brightness effects on LAI and APAR estimation. In: *Proceedings of IGARSS '89. 12th Canadian symposium on remote sensing, Vancouver, Canada, July 10–14, 1989* (vol. 3, 1355–1358).

Baret, F., Jacquemoud, S., Guyot, G., & Leprieur, C. (1992). Modeled analysis of the biophysical nature of spectral shifts and comparison with information content of broad bands. *Remote Sensing of Environment*, *41*, 133–142.

Blackburn, G. A. (1998). Quantifying chlorophylls and carotenoids at leaf and canopy scales: an evaluation of some hyperspectral approaches. *Remote Sensing of Environment*, *66*, 273–285.

Bonham-Carter, G. F. (1988). Numerical procedures and computer program for fitting an inverted Gaussian model to vegetation reflectance data. *Computers & Geosciences*, *14*, 339–356.

Bouman, B. A. M. (1992). Linking physical remote sensing models with crop growth simulation models, applied for sugar beet. *International Journal of Remote Sensing*, *13*, 2565–2581.

Bouman, B. A. M. (1995). Crop modelling and remote sensing for yield prediction. *Netherlands Journal of Agricultural Science*, *43*, 143–161.

Broge, N. H., Hvidberg, M., Hansen, B. U., Andersen, H. S., & Nielsen, A. A. (1997). Analyses of spectral–biophysical relationships for a wheat canopy. In: *Proceedings of the 3rd international airborne remote sensing conference and exhibition, Copenhagen, Denmark, July 7–10, 1997* (vol. 2, pp. 373–379). Ann Arbor, MI, USA: ERIM International.

Broge, N. H., & Leblanc, E. (2001). Comparing prediction power and stability of broadband and hyperspectral vegetation indices for estimation of green leaf area index and canopy chlorophyll density. *Remote Sensing of Environment*, *76*, 156–172.

Campbell, R. J., Mobley, K. N., Marini, R. P., & Pfeiffer, D. G. (1990). Growing conditions alter the relationship between SPAD-501 values and apple leaf chlorophyll. *HortScience*, *25*, 330–331.

Clark, R. N., & Roush, T. L. (1984). Reflectance spectroscopy: quantitative analysis techniques for remote sensing applications. *Journal of Geophysical Research*, *89*, 6329–6340.

Collins, W. (1978). Remote sensing of crop type and maturity. *Photogrammetric Engineering and Remote Sensing*, *26*, 43–55.

Dawson, T. P., & Curran, P. J. (1998). A new technique for interpolating the red edge position. *International Journal of Remote Sensing*, *19*, 2133–2139.

Demetriades-Shah, T. H., Steven, M. D., & Clark, J. A. (1990). High resolution derivative spectra in remote sensing. *Remote Sensing of Environment*, *33*, 55–64.

Elvidge, C. D., & Chen, Z. (1995). Comparison of broad-band and narrow-band red and near-infrared vegetation indices. *Remote Sensing of Environment*, *54*, 38–48.

Filella, I., & Peñuelas, J. (1994). The red edge position and shape as indicators of plant chlorophyll content, biomass and hydric status. *International Journal of Remote Sensing*, *15*, 1459–1470.

Gilabert, M. A., Gandia, S., & Melia, J. (1996). Analyses of spectral–biophysical relationships for a corn canopy. *Remote Sensing of Environment*, *55*, 11–20.

Gitelson, A. A., & Merzlyak, M. N. (1996). Signature analysis of leaf reflectance spectra: algorithm development for remote sensing of chlorophyll. *Journal of Plant Physiology*, *148*, 494–500.

Gitelson, A. A., Merzlyak, M. N., & Lichtenthaler, H. K. (1996). Detection of red edge position and chlorophyll content by reflectance measurements near 700 nm. *Journal of Plant Physiology*, *148*, 501–508.

Goel, N. S. (1989). Inversion of canopy reflectance models for estimation of biophysical parameters from reflectance data. In: G. Asrar (Ed.), *Theory and applications of optical remote sensing* (pp. 205–251). New York: John Wiley & Sons.

Hansen, J. G. (1991). Use of multispectral radiometry in wheat yellow rust experiments. *Bulletin OEPP/EPPO*, 651–658.

Hinzman, L. D., Bauer, M. E., & Daughtry, C. S. T. (1986). Effects of nitrogen fertilization on growth and reflectance characteristics of winter wheat. *Remote Sensing of Environment*, *19*, 47–61.

Horler, D. N. H., Dockray, M., & Barber, J. (1983). The red edge of plant leaf reflectance. *International Journal of Remote Sensing*, *4*, 273–288.

Huete, A. R. (1989). Soil influences in remotely sensed vegetation-canopy spectra. In: G. Asrar (Ed.), *Theory and applications of optical remote sensing* (pp. 107–141). New York: Wiley.

Inskeep, W. P., & Bloom, P. R. (1985). Extinction coefficients of chlorophyll *a* and *b* in *N*,*N*-dimethylformamide and 80% acetone. *Plant Physiology*, *77*, 483–485.

Irons, J. R., Weismiller, R. A., & Petersen, G. W. (1989). Soil reflectance. In: G. Asrar (Ed.), *Theory and applications of optical remote sensing* (pp. 66–106). New York: Wiley.

ISSS Working Group RB. (1998). In: E. M. Bridges, N. H. Batjes, & F. O. Nachtergaele (Eds.), *World reference base for soil resources: atlas* (79 pp.). Leuven: ISRIC_FAO_ISSS, ACCO.

Jackson, R. D., Clarke, T. R., & Moran, M. S. (1992). Bidirectional calibration results for 11 spectralon and 16 $BaSO_4$ reference reflectance panels. *Remote Sensing of Environment*, *40*, 231–239.

Jacobsen, B. H., Petersen, B. M., Berntsen, J., Boye, C., Sørensen, C., Søgaard, C. G., & Hansen, J. P. (1998). *An integrated economic and environmental farm simulation model (FASSET)*. Danish Institute of Agricultural and Fisheries Economics, Report No. 102, Copenhagen, Denmark, 152 pp.

Jordan, C. F. (1969). Derivation of leaf area index from quality of light on the forest floor. *Ecology*, *50*, 663–666.

Kim, M. S., Daughtry, C. S. T., Chappelle, E. W., & McMurtrey, J. E. (1994). The use of high spectral resolution bands for estimating absorbed photosynthetically active radiation (APAR). In: *Proceedings of the 6th international symposium on physical measurements and signatures in remote sensing* (pp. 299–306). France: Val d'Isere.

Kruse, F. A. (1988). Use of airborne imaging spectrometer data to map minerals associated with hydrothermally altered rocks in the Northern Grapevine Mountains, Nevada and California. *Remote Sensing of Environment*, *24*, 31–51.

Lichtenthaler, H. K., Gitelson, A. A., & Lang, M. (1996). Non destructive determination of chlorophyll content of leaves of a green and an aurea mutant of tobacco by reflectance measurements. *Journal of Plant Physiology*, *148*, 483–493.

Major, D. J., Baret, F., & Guyot, G. (1990). A ratio vegetation index adjusted for soil brightness. *International Journal of Remote Sensing*, *11*, 727–740.

Manetas, Y., Grammatikopoulus, G., & Kyparissis, A. (1998). The use of the portable, non-destructive, SPAD-502 (Minolta) chlorophyll meter with leaves of varying trichome density and anthocyanin content. *Journal of Plant Physiology*, *153*, 513–516.

Markwell, J., Ostermann, J. C., & Mitchell, J. L. (1995). Calibration of the Minolta SPAD-502 leaf chlorophyll meter. *Photosynthesis Research*, *46*, 467–472.

Mauser, W., & Bach, H. (1995). Imaging spectroscopy in hydrology and agriculture — determination of model parameters. In: J. Hill, & J. Megier (Eds.), *Imaging spectrometry — a tool for environmental observations* (pp. 261–283). Dordrecht, The Netherlands: Kluwer Academic Publishing.

Miller, J. R., Hare, E. V., & Wu, J. (1990). Quantitative characterization of the vegetation red edge reflectance. *International Journal of Remote Sensing*, *11*, 1755–1773.

Monje, O. A., & Bugbee, B. (1992). Inherent limitations of nondestructive chlorophyll meters: a comparison of two types of meters. *HortScience*, *27*, 69–71.

Moran, M. S., Maas, S. J., & Pinter Jr., P. J. (1995). Combining remote sensing and modeling for estimating surface evaporation and biomass production. *Remote Sensing Review*, *12*, 335–353.

Moran, R. (1992). Formulae for determination of chlorophylleous pigments extracted with *N*,*N*-dimethylformamide. *Plant Physiology*, *69*, 1376–1381.

Moran, R., & Porath, D. (1980). Chlorophyll determination in intact tissues using *N*,*N*-dimethylformamide. *Plant Physiology*, *65*, 478–479.

Moulin, S., & Guérif, M. (1999). Impacts of model parameter uncertainties on crop reflectance estimates: a regional case study on wheat. *International Journal of Remote Sensing*, *20*, 213–218.

Myneni, R. B., & Williams, D. L. (1994). On the relationship between FAPAR and NDVI. *Remote Sensing of Environment*, *49*, 200–211.

Olesen, J. E., Petersen, B. M., Berntsen, J., Hansen, S., Jamieson, P. D., & Thomsen, A. G. (2001). Comparison of methods for simulating effects of nitrogen on green area index and dry matter growth in winter wheat. *Field Crops Research* (accepted for publication).

Osman, A. M., Goodman, P. J., & Cooper, J. P. (1977). The effects of nitrogen, phosphorus, and potassium on rates of growth and photosynthesis of wheat. *Photosynthetica*, *11*, 66–75.

Pearson, R. L., & Miller, L. D. (1972). Remote mapping of standing crop biomass for estimation of the productivity of the short-grass prairie, Pawnee National Grasslands, Colorado. In: *Proceedings of the 8th International Symposium on Remote Sensing of Environment, ERIM International* (pp. 1357–1381) (Ann Arbor, MI, USA).

Pinar, A., & Curran, P. J. (1996). Grass chlorophyll and the reflectance red edge. *International Journal of Remote Sensing*, *17* (2), 351–357.

Pinter Jr., P. J., Jackson, R. D., Ezra, C. E., & Gausman, H. W. (1985). Sun-angle and canopy-architecture effects on the spectral reflectance of six wheat cultivars. *International Journal of Remote Sensing*, *6* (12), 1813–1825.

Porra, R. J., Thompson, W. A., & Kriedemann, P. E. (1989). Determination of accurate extinction coefficients and simultaneous equations for assaying chlorophylls a and b extracted with four different solvents: verification of the concentration of chlorophyll standards by atomic absorption spectroscopy. *Biochimica Biophysica Acta*, *975*, 384–394.

Press, W. H., Flannery, B. P., Teukolsky, S. A., & Vetterling, W. T. (1989). *Numerical recipes in Pascal. The art of scientific computing*. New York: Cambridge University Press (759 pp.).

Qi, J., Chehbouni, A., Huete, A. R., Kerr, Y. H., & Sorooshian, S. (1994). A modified soil adjusted vegetation index. *Remote Sensing of Environment*, *48*, 119–126.

Reujean, J., & Breon, F. (1995). Estimating PAR absorbed by vegetation from bidirectional reflectance measurements. *Remote Sensing of Environment*, *51*, 375–384.

Richardson, A. J., & Wiegand, C. L. (1977). Distinguishing vegetation from soil background information. *Photogrammetric Engineering and Remote Sensing*, *43*, 1541–1552.

Rouse, J. W., Haas, R. H., Schell, J. A., Deering, D. W., & Harlan, J. C. (1974). *Monitoring the vernal advancement of retrogradation of natural vegetation.* NASA/GSFC, Type III, Final Report, Greenbelt, MD, USA. (pp. 1–371).

SAS Institute. (1988). *SAS/STAT user's guide* (Release 6.03 edition). Cary, NC, USA: SAS.

Schaper, H., & Chacko, E. K. (1991). Relation between extractable chlorophyll and portable chlorophyll meter readings in leaves of eight tropical and subtropical fruit-tree species. *Journal of Plant Physiology*, *138*, 674–677.

Thomas, J. R., & Gausman, H. W. (1977). Leaf reflectance vs. leaf chlorophyll and carotenoid concentrations for eight crops. *Agronomy Journal*, *69*, 799–802.

Thomsen, A., Schelde, K., Heidmann, T., & Hougaard, H. (1997). Mapping field variability in crop development and water balance within a field with highly variable soil conditions. In: J. V. Stafford (Ed.), *Precision agriculture '97: papers presented at the first European conference on precision agriculture, Warwick University Conference Centre, UK, September 7–10* (pp. 189–196). Warwick University Conference Centre, UK: BIOS Scientific Publishers Ltd.

Welles, J. M., & Norman, J. M. (1991). Instrument for indirect measurement of canopy architecture. *Agronomy Journal*, *83*, 818–825.

Wiegand, C. L., Maas, S. J., Aase, J. K., Hatfield, J. L., Pinter Jr., P. J., Jackson, R. D., Kanemasu, E. T., & Lapitan, R. L. (1992). Multisite analyses of spectral–biophysical data for wheat. *Remote Sensing of Environment*, *42*, 1–21.

Yadava, U. L. (1986). A rapid and nondestructive method to determine chlorophyll in intact leaves. *HortScience*, *21*, 1449–1450.

Zadoks, J. C., Chang, T. T., & Konzak, C. F. (1974). A decimal code for the growth stages of cereals. *Weed Research*, *14*, 415–421.